THE ACCURACY OF AUTOMATED VOLUME MEASUREMENTS IN OPTICAL FLUORESCENCE MICROSCOPY

Felix Martin MARGADANT
Institute of Biomedical Engineering
Gloriastrasse 35
8092 Zürich, Switzerland

Abstract

Quantitative fluorescence microscopy resides on the circumstance that under not too strong illumination, the fluorescent light emitted by a fluorophore - a dye with specific fluorescent properties - is first order proportional to both the light flux and the dye quantity [WEL94]. There are two aspects of quantification, the spatial measurements and the dosimetry of fluorescence, called fluorometry. The achievable accuracy in the disciplines depends of the spatial resolving power - the *resolution* - and the optical *dynamics* or *range* of the light sensors. Most texts deal with each topics individually, though it easy to proof that they closely interact and even cannot be defined separately [BRA91], [CAS93], [WIL93].

Here we discuss the problems and the restrictions of automated geometric measurements due to fluorescence processes. Volume measurements have been chosen because they allow for more computational improvement compared to distance determination and they are mathematically easier accessible than area descriptions. Automated measurement means that the volume boundaries are determined by a segmentation algorithm. From the formal point of view this has the advantage that one can describe how the instrumental deviations and determination errors superimpose.

Digital imaging

To analytically describe the resolving power of light microscopes, single lens models and far-field approximations are used. The theories describe real-world microscopes almost perfectly, and commercial systems closely reach the theoretical diffraction limit [GU96], [KIN88], [OFF88], [WIL93]. For digital microscopy therefore it is wise to choose the discretization step - the digital resolution - to be equal to the diffraction limit. Since two bright structures can be distinguished when they are apart twice the diffraction limit, this setting satisfies Shannon's sampling theorem. The continuos intensity distribution $I(\bar{x})$ is sampled into the discrete voxel values $v(\bar{i}) := \frac{1}{\|\sigma\|} \iiint_{\sigma(\bar{i})} I(\bar{x}) d\bar{x}$ (eq1),

where $\sigma(\bar{i})$ is the environment centered around a discrete vector $\bar{i}$ with the dimension of the sampling distances, and the normalization factor is the volume of the environment.

The resolution differs significantly in lateral- Δ_l and depth-direction Δ_d. Since in each axis convex volumes feature two boundaries, the volumetric resolution of the instrument may be defined as $\Delta^{(0)}v := 2\Delta_d(2\Delta_l)^2$ which is a almost useless definition since - in contrast to the linear resolution - the volumetric accuracy depends on the volume size. $\Delta^{(0)}v$ serves just as an instrument parameter.

Localization

Localization is the precision at which a boundary of two objects can be determined, it therefore is an instrument as well as a specimen property. Perpendicular to the boundary of two adjacent objects of constant intensities v_0 and v_1, there is at most one voxel with an intensity not equal to v_0 or v_1, the transition-voxel. The boundary can be precisely located, thoroughly independent of the resolution. Fig. 1 illustrates this case in one dimension. x_0 is the coordinate of the transition voxel with intensity v_T. According to eq1, $v_T = dx \cdot v_0 + (1-dx) \cdot v_1$ (eq2a) and therefore, the transition lies at $x_0 + dx = x_0 + \frac{v_T - v_1}{v_0 - v_1}$ (eq2).

Since the localization is unlimited, the volumetric error is zero.
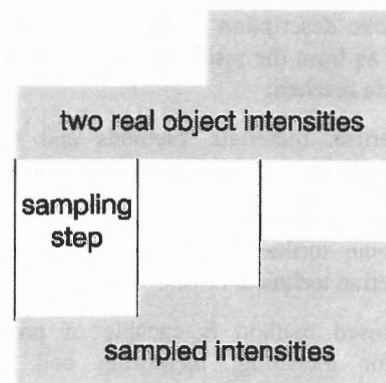
fig. 1
noise free sampling

Noise

Real measurements impose a noise figure on the voxel values. We reduce the known noise characteristics to a mean noise amplitude n which is equal to the squareroot of the variance induced by the noise, but we respect that noise variance is linear proportional to the image intensity [PAW94]. Even small noise energies introduce major conceptual changes to the localization approaches. E.g. for eq2 we obtain $v_T = dx \cdot v_0 + (1 - dx) \cdot v_1 \pm n$

and therefore $dx = \dfrac{v_T \pm n - v_1}{v_0 - v_1}$ and therefore a

mean localization error $\delta x = \left| \dfrac{n}{v_0 - v_1} \right|$ (eq3). This

gets critical for $\delta x > \frac{1}{2}, n > \frac{1}{2} |v_0 - v_1|$, because then the presumption that there is one transition-voxel becomes invalid. Filtering methods can be applied to get a lower noise figure at the expense of resolution. It is, however, unsolved how to describe the impact on resolution for a general class of filters [CAS96]. Therefore we used the approach of multipoint statistics to simulate an image, as if it was recorded at lower resolution [MAR96_2]. We could show that you get well defined transition again, if the boundary surface of two objects covers more than k voxels and $n < \frac{1}{2} \sqrt{k} |v_0 - v_1|$ (eq4). Further, some advanced filter techniques perform better and achieve the goal for $n < \alpha \sqrt{k} |v_0 - v_1|$ with $\frac{1}{2} < \alpha < 1$. Both results have to be considered unfortunate, because the resolution now depends on the instrument, the noise and, additionally, on the size of objects and the localization method. Larger objects have better defined boundaries, as it is even proven for pure optical observations [KIN88].

Filter masks

The so called *size of the filter mask*, [CAS96] is the number of voxels involved in the multipoint statistics. From the noise pattern one can immediately derive, how reliable the assignment to a certain level (here either v_0 or v_1). Fig. 2 illustrates the wrong-assignment probability for two adjacent objects which differ in brightness by the noise level. λ is the mask size.

decision error
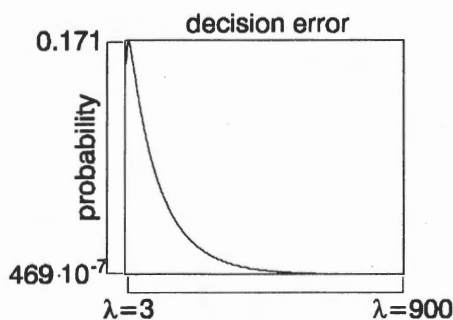
fig. 2
reliability vs. filter mask size

There is no immediate criterion how large the mask shall be. If we look at subvolumes of linear dimension k, k^3 voxels are involved, the surface area is stretched k^2 times, but as soon k is large enough so that eq4 is satisfied, δx becomes k times smaller - for voxels which are now k times larger in diameter. Therefore eq3 provides no hint how the mask shall be chosen, there is solely a lower bound for the size due to eq4.

Split strategy

The approach induces two classes of voxels per single object: inner- and surface-voxels. The localization of the surface voxels is independent of the filter size, and the detection probability of the inner voxels increases with mask size, according to fig. 2. So, the volume assignment improves for coarse masks. The size of the filter mask therefore is only limited by the surface mesh defined by the mask: the more extended the filter mask is chosen, the fewer sampling vertices on the surface can be defined and the curvature of the surfaces is less well defined. This corresponds to a second order shape parameter added to the linear polyhedron which forms the object boundary, therefore its influence is linear to the mask diameter and not its area. The volumetric error therefore increases linearly to the mask diameter, whereas the assignment error for the inner voxels decreases exponentially with the mask volume. The global minimum is given by fig. 2, and it varies substantially with the absolute size of the object under consideration.

Smaller objects cannot be filtered as severely as large ones. This may lead to strange effects, such as that the absolute volumetric error for larger objects can get smaller than for smaller ones. For a noise level which is k times stronger than the separation of the objects, large objects may reach up to k times the diameter of small ones and will still be measured at a higher absolute volumetric accuracy.

Microscopes

Microscopes add one important aspect: a high degree of inhomogenity. Microscopic images are falsified by an extended set of influences. The most striking ones are discussed in [SCA96] - the medium and the specimen defocus the light and blur it - the so called *aberration* -, and the subsequent depth discrimination optics cuts off the blurred light which leads to a strong loss of image intensities for the deeper layers of the specimen. The strong laser light deteriorates the fluorophores which results in exponential signal loss over time, and finally, the specimen absorbs light and therefore attenuates the signal. The last influence is the most complicated one to compensate for [MAR96], [ROE91], but not the strongest one. Even for an isotropic specimen with constant refraction and attenuation, one obtains a very complex light-loss pattern in the depth

direction $\left(\dfrac{1}{d+N(z-z_0)^2}\right)\left(\left(\dfrac{-a}{z}\right)E_i(\dfrac{-a}{z})-e^{-\frac{a}{z}}(1-\dfrac{a}{z})\right)\cdot\left(e^{-z\cdot A}\right)$

(eq5), where z is the depth variable [MAR96_2]. Here the first bracket represents the aberration - N is collective constant for the wavelength and the refractive index, d is normalization index, and z_0 is the depth of focus-, the second factor stands for the attenuation - a is the damping constant - and the last one is the deterioration factor - A is a constant for the light intensity and the time-per-section. Fig. 3 shows a microscopic section degraded this way.
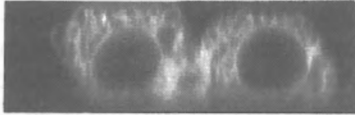
fig. 3
depth degrade confocal image

It is inadequate to evaluate eq5 to investigate the influence on the localization. Instead, we assume an *amplification error* q at the depth of interest. Again we use a modified eq2a
$$v_T\cdot q = dx\cdot v_0 + (1-dx)\cdot v_1$$ and get
$\delta x = (1-q)\dfrac{v_T}{v_0-v_1}$ (eq6). Considering that q may go down to 0.2 [MAR96], this disables simple detection methods such as thresholding.

Image restoration
Since the image formation processes in the microscope are known, the quantitative image reconstruction basically is possible. [BAC94], [MAR96], [ROE91] elucidate certain aspects of microscopic image restoration. At our location we developed a software package called QUASIA-3D (**qu**antitative **s**ystem for **i**mage **a**cquisition in **3D** microscopy) that takes into account all of the previously mentioned influences and a few more ones. A restoration run is depicted in fig. 4.
Thereby, the q factor can be eliminated, however, the noise level increases inverse proportional to q. With $\dfrac{1}{\left(q+\varepsilon\cdot q^2\right)}$ (eq7), more precisely, but ε is a rather small constant - about 2% for 20 sections.

The improvement for thresholding is invaluable - for a real specimen, the errors decreased to about 50% from some 300% for the unprocessed image.
Even edge detector operators like [CAN86] gain efficiency - the noise level increases linear to q^{-1}, but the count of available reference voxels goes up stronger than q^{-2}, because the image is equalized.
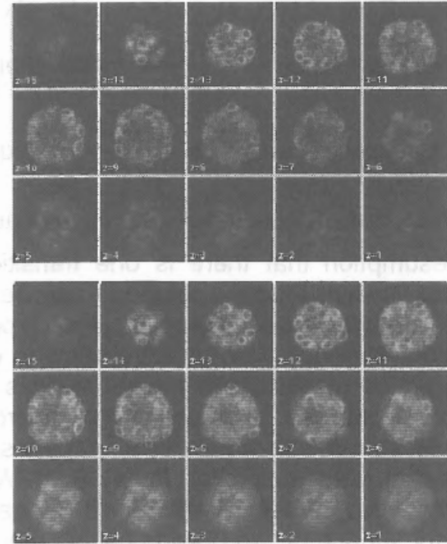
fig. 4
original and reconstructed image dataset

Conclusions
It is possible to improve the performance of all general filter procedures in the context of localization, by prior application of quantitative reconstruction, even, if the improvement for complex filters cannot be quantified.
Simple multipoint-statistics give a lower bound how rewarding image restoration in advance to segmentation is. For severely degraded microscopic images a deviation due to the light loss of up to 400% can be expected, for which restoration improves localization somewhat worse than a factor of 4, as eq7 lets expect.
Splitting the volumetry in surface and core voxels brings - aside from easier computation - a true criterion how filtering shall be chosen and a quantitative estimate of the to be expected errors due to noise.

References

[BAC94]

Three-Dimensional Volume Reconstruction in Confocal Microscopy: Practical Considerations
R.Baccalao, A.Garfinkel
Three-Dimensional Confocal Microscopy 1994

[BRA91]

Basic Measurement Techniques for Light Microscopy
S.Bradbury, P.J.Evennett, H.Haselmann, H.Piller
RMS Microscopy Handbooks, Oxford Science Publications

[CAN86]

A Computational Approach to Edge Detection
J.Canny
IEEE Transactions on Pattern Analysis and Machine Intelligence, p. 679, 1986

[CAS93]

Resolution and Sampling Requirements for Digital Image Processing, Analysis and Display
K.R.Castleman
Electronic Light Microscopy 93

[CAS96]

Digital Image Processing
K.R.Castleman
Prentice-Hall Inc.

[GU96]

Principles of three-dimensional imaging in confocal microscopes
Min Gu
Singapore (etc.) : World Scientific, cop. 1996

[HAM88]

Excentration errors combined with wavefront aberration in a coherent scanning microscope
A.M.Hammed
SPIE Proceedings 1988

[HEL88]

Spherical Aberration in Confocal Microscopy
T.Hellmuth, P.Seidel, A.Siegel
SPIE Proceedings 1988

[KIN88]

Imaging theory for the scanning optical microscope
G.S.Kino, C-H.Chou and G.Q.Xiao
SPIE Proceedings 1988

[MAR96]

A precise light attenuation correction for confocal scanning microscopy with O(n4/3) computing time and O(n) memory requirements for n voxels
F. Margadant, T. Leemann, P. Niederer
Journal of Microscopy, Vol. 181, Pt 3, May 1996

[MAR96_2]

Visualization of noisy and weak structures at the resolution limit
(in German: Visualisierung schwacher verrauschter Strukturen an der Auflösungsgrenze)
F. Margadant
Biomedical Techniques Europe, Sep. 1996

[MEY92]

Integrals and Gradients of Images
F.Meyer
Image Algebra and Morphological Image Processing III, SPIE 1992

[OFF88]

Axial resolution of a confocal scanning optical microscope
M.J.Offside, C.W.See and M.G.Somekh
SPIE Proceedings 1988

[PAW94]
Sources of Noise in Three-Dimensional Microscopical Data Sets
.J.B.Pawley
Three-Dimensional Confocal Microscopy 1994

[PIT93]
Digital Image Processing Algorithms
J.Pitas
Prentice International Series 1993

[ROE91]
An FFT-based Method for Attenuation Correction in Fluorescence Confocal Microscopy
Roerdink, J.B.T.M., Bakker, M.
Department for Analysis, Algebra and Geometry Amsterdam: CWI 1991

[SCA96]
Dispersion, Aberration and Deconvolution in Multi-Wavelength Fluorescence Images
B.A.Scalettar, J.R.Swedlow, J.W.Sedat, D.A.Agard
Journal of Microscopy, Vol. 182, 1996

[WEL94]
Fluorescent Labels for Confocal Microscopy
S.Wells, I.Johnson
Three-Dimensional Confocal Microscopy 1994

[WIL93]
Image Formation in Confocal Microscopy
T.Wilson
Electronic Light Microscopy 93